

Hadronic Final States in e^+e^- -Interactions and their Relevance to Cosmic Rays

Claus Grupen

University of Siegen, Germany

ABSTRACT

Elementary particle aspects using beams from accelerators and cosmic rays are compared. An important feature in high energy physics is particle identification in the final state. This technique is used to describe global features of e^+e^- -annihilations such as multiplicities and multiplicity distributions of charged hadrons and the relative fractions of pions, kaons and protons. Also the characteristic properties of quark and gluon jets and scaling violation in e^+e^- -interactions are discussed.

INTRODUCTION

Cosmic ray experiments investigating problems of high energy physics are always fixed target experiments. This implies the disadvantage that only a small fraction of the energy of the incident particle can be used for the creation of new particles while the major part is used to boost the interaction products into the forward direction.

For a target of mass m and an energy of the incident particle E_{lab} the center-of-mass energy squared s is calculated to be

$$s = 2mE_{\text{lab}}, \quad (1)$$

as long as $E_{\text{lab}} \gg mc^2$. This leads to a center-of-mass energy of 1 TeV for a cosmic ray particle of $5 \cdot 10^{14}$ eV hitting a proton target.

The best use of the energy of the particle at accelerators is made with the technique of storage rings. Two particles of 500 GeV each achieve the same center-of-mass energy of 1 TeV in a head-on collision. Here the full energy of the particles can be used for new particle creation.

The particle accelerators in operation and those in construction will cover equivalent laboratory energies up to 10^{17} eV. The energy domain beyond 10^{17} eV will

be reserved for high energy physics with cosmic rays. The problem there, however, is that the rates are extremely low. But elementary particle physics is only one aspect of cosmic rays, the other possibly more important one is astronomy and astrophysics.

EXPERIMENTAL TECHNIQUES IN e^+e^- COLLIDER-EXPERIMENTS

The fundamental process of hadron production in e^+e^- -collisions can be subdivided into five steps:

- (i) The electron and positron annihilate into a virtual gauge boson, γ or Z ; this process is entirely described by the standard model of electroweak interactions (see Fig. 1, [1, 2]).
- (ii) The photon or Z produce a quark-antiquark pair. This transition is also understood in the framework of the standard model.
- (iii) The quarks initiate a quark-gluon cascade. As long as the virtuality of the partons is larger than a certain cut-off value (typically 1 GeV) this parton shower can be calculated in perturbative quantum chromodynamics (QCD).
- (iv) The transition of partons to primary hadrons cannot be calculated in QCD but rather requires phenomenological models of the hadronization process.
- (v) Finally the primary hadrons or their decay products ($\rho^0 \rightarrow \pi^+\pi^-$; $\Lambda \rightarrow p\pi^-$; $\eta \rightarrow \gamma\gamma$; ...) can be recorded in the detector [3].

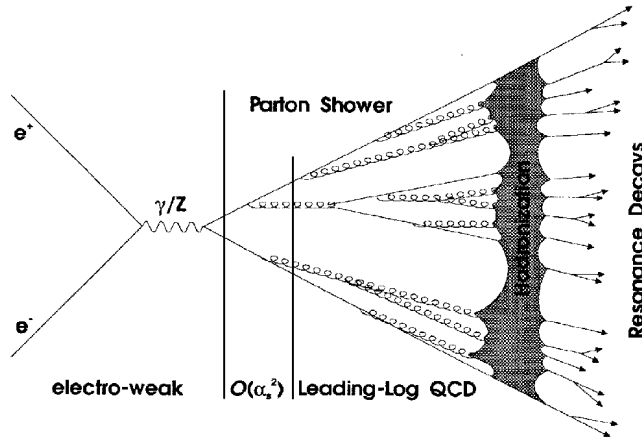


Figure 1: Fundamental processes of hadron production in e^+e^- annihilation [1, 2].

It is desirable to identify all particles in the hadronic final state. Several techniques can be used to achieve this [4]:

- (i) The ionization loss dE/dx provides information on the charge Z of the particle (usually $Z = 1$ in e^+e^- collisions) and its velocity β .
- (ii) Ring-imaging Cherenkov counters (RICH) equally determine Z and β .
- (iii) Electromagnetic and hadron calorimeters distinguish between e^+ , e^- , γ on the one hand and π , K , p , n on the other hand on the basis of the characteristically different shower profiles of the particles.
- (iv) Muons are identified by their penetration through e.g. the hadron calorimeter.
- (v) Particles which decay after a very short path length are identified by the reconstruction of their invariant mass from their decay products.
- (vi) Finally an accurate momentum measurement in a high resolution spectrometer $p = \gamma m_0 \beta c$ fixes the particle mass, if its velocity is known.

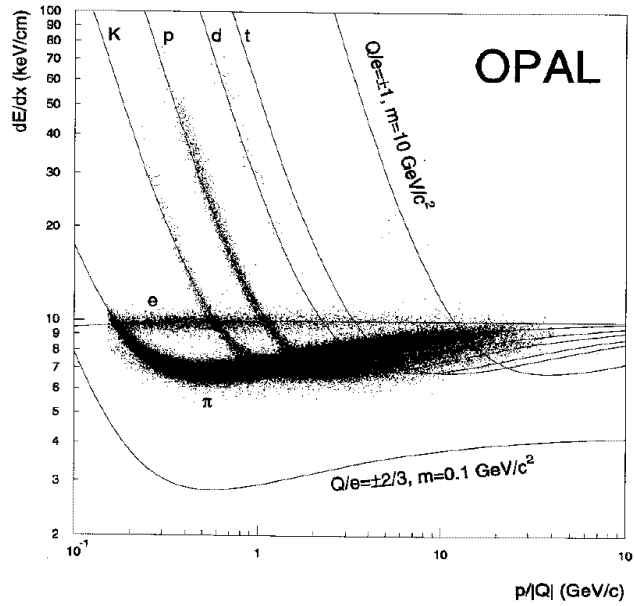


Figure 2: Energy loss curves for electrons, pions, kaons, protons and deuterons in the OPAL central tracking chamber [6]. The diagram also shows that exotic particles are not produced in e^+e^- interactions.

Fig. 2 shows the energy loss curves for electrons, pions, kaons, protons, deuterons and tritons in the OPAL tracking chamber [5, 6]. Below momenta of 1 GeV/c a clear separation between the different particle species is possible. Also in the relativistic rise region a certain particle identification power is obtained. This can be substantially improved upon by making use of additional information from calorimeters and/or Cherenkov counters.

MULTIPLICITIES AND MULTIPLICITY DISTRIBUTIONS

At first glance the determination of the charged multiplicity in hadronic final states seems to be easy. However, the loss of particles at low momentum and imperfections of track reconstruction in collimated jets requires an unfolding procedure to arrive at the true multiplicity from the observed one [7].

Fig. 3 shows the charged particle multiplicities observed in e^+e^- -interactions at different center-of-mass energies (after [2]). The data can be compared to various parametrizations [8]. The formulae given in the following equations (2) - (7) are based on fits to data obtained in the energy range from $\sqrt{s} = 2$ GeV to $\sqrt{s} = 91$ GeV. Recently obtained results at $\sqrt{s} = 133$ GeV can be used to judge on the quality of the parametrization [9, 10, 11, 12].

A simple power law

$$\langle n_{\text{ch}} \rangle = a \cdot s^b \quad (2)$$

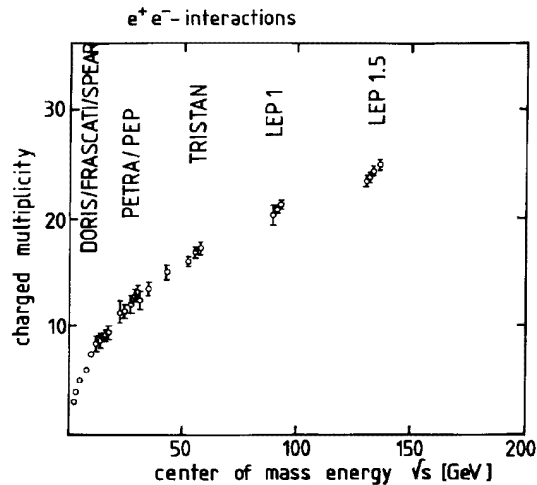


Figure 3: Charged multiplicities in e^+e^- interactions from various e^+e^- collider experiments (after [2]).

motivated by phase space arguments does not fit the new data well ($a = 2.22$; $b = 0.252$). Fermi's idea applied to discrete distributions

$$\langle n_{\text{ch}} \rangle = \beta \cdot s^\alpha - 1 \quad (3)$$

describes the data rather well ($\beta = 2.979$; $\alpha = 0.222$), and so does the frequently used empirical relation

$$\langle n_{\text{ch}} \rangle = a + b \cdot \ln s + c \ln^2 s \quad (4)$$

($a = 3.297$; $b = -0.394$; $c = 0.263$). The QCD inspired parametrization based on leading-log approximation

$$\langle n_{\text{ch}} \rangle = a + b \cdot e^{c \sqrt{\ln(s/Q_0^2)}} \quad (5)$$

with $a = 2.418$; $b = 0.113$; $c = 1.712$ and $Q_0 = 1$ GeV cannot really account for the 133 GeV data, but the inclusion of next-to-leading-log expressions in QCD provides a good description of the high energy data

$$\langle n_{\text{ch}} \rangle = a \cdot \alpha_s^b \cdot e^{c/\sqrt{\alpha_s}} \quad (6)$$

with $a = 0.065$; $b = 0.49$; $c = 2.27$ and

$$\alpha_s = \frac{4\pi}{\beta_0 \ln s / \Lambda^2} - \frac{4\pi\beta_1 \ln \ln s / \Lambda^2}{\beta_0^3 \ln^2 s / \Lambda^2} \quad (7)$$

with $\beta_0 = 7.67$; $\beta_1 = 38.67$ and $\Lambda = 136$ MeV. α_s is the running coupling constant of strong interactions.

For the same center-of-mass energy the charged particle multiplicity in proton-proton collisions is smaller compared to e^+e^- -collisions. This relates to the fact that in e^+e^- -interactions the full center-of-mass energy is available for particle production while in pp-collisions one deals with quark-quark scattering, and the quark-quark system carries only a fraction of the proton-proton center-of-mass energy [13].

The multiplicity distribution (Fig. 4) exhibits KNO-scaling when plotted in the normalized variables $\Psi(z) = \langle n_{\text{ch}} \rangle \cdot P(n_{\text{ch}})$ and $z = n_{\text{ch}} / \langle n_{\text{ch}} \rangle$, where $P(n_{\text{ch}})$ is the probability to observe n_{ch} hadrons for an average of $\langle n_{\text{ch}} \rangle$ [7]. For a center-of-mass energy of $\sqrt{s} = 91$ GeV the multiplicity distribution is best described by a log-normal distribution, but also the negative binomial distribution fits the data quite well.

At low momenta (≤ 1 GeV/c) the final state is dominated by pions ($\geq 85\%$). The particle composition changes significantly for higher momenta. Around $p = 10$ GeV/c there are about 60 % pions, 30 % kaons and 10 % protons.

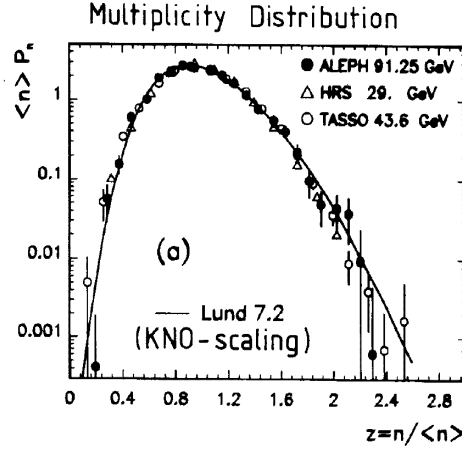


Figure 4: Unfolded charged multiplicity distribution in KNO form comparing data from ALEPH, HRS and TASSO [7]

The high statistics also allows to identify the production of strange and charmed baryons, such as Σ , Ξ and Ω . For example, the Ω^- multiplicity is of the order of 0.001 per event at $\sqrt{s} = 91$ GeV.

PROPERTIES OF QUARK AND GLUON JETS

In three-jet events, where one of the primary quarks radiates an energetic gluon it is possible, to distinguish the gluon jet from the quark jets. If one selects $q\bar{q}g$ events where the quarks are either charm or bottom quarks one may find in these quark jets evidence for long-lived hadrons (B-mesons or D-mesons). Experimentally one looks for decay vertices of B or D-mesons displaced from the primary vertex. In the gluon jet the production of B or D-mesons is rather unlikely because the charm and bottom quarks are too heavy. Consequently in three-jet events with evidence for long-lived hadrons in two jets the third jet must have been initiated by a gluon.

The sample of tagged three-jet events can now be used to search for differences between quark and gluon jets. It turns out that gluon jets are wider and contain also more particles than quark jets. The increase in particle multiplicity in gluon jets is concentrated at low hadron momenta causing the fragmentation function of gluons to be softer than the quark fragmentation function (e.g. [14]).

SCALING VIOLATIONS IN e^+e^- -INTERACTIONS

Feynman-scaling states that in the quark-parton model the normalized inclusive cross-section

$$\frac{1}{\sigma_{\text{tot}}} \frac{d\sigma}{dx} \quad \text{with} \quad x = \frac{E_{\text{hadron}}}{E_{\text{beam}}} = \frac{2 E_{\text{hadron}}}{\sqrt{s}} \quad (8)$$

does not depend on the center-of-mass energy. Feynman-scaling is known to be violated, and the evidence for that comes from accelerator and cosmic ray experiments. The reason for this scaling violation originates from gluon radiation which leads to a dependence of $\frac{1}{\sigma_{\text{tot}}} \frac{d\sigma}{dx}$ on the center-of-mass energy.

These scaling violations come about because with increasing \sqrt{s} more phase space for gluon radiation and thus final state particle production becomes available leading to a softer x -distribution at higher center-of-mass energies.

The inclusive cross-section for

$$e^+e^- \rightarrow \text{hadron} + \text{anything} \quad (9)$$

has been measured for center-of-mass energies between 22 GeV and 91 GeV [2, 15]. The fragmentation functions get softer at higher values of \sqrt{s} . This is clearly seen in Fig. 5 where the ratio of the inclusive cross-sections at 91 GeV and 22 GeV is shown [15]. Higher center-of-mass energies lead to an enhancement at low momenta and a depletion at high hadron momenta.

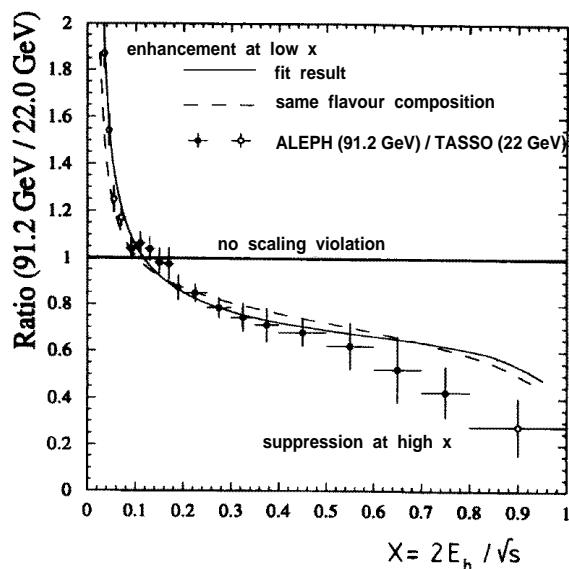


Figure 5: Ratio of inclusive cross-sections at $\sqrt{s} = 91.2\text{ GeV}$ and $\sqrt{s} = 22\text{ GeV}$ [15].

CONCLUSIONS

Colliders can reach equivalent laboratory energies of $E_{\text{lab}} = 10^{17}$ eV. The domain beyond this energy is reserved for cosmic rays.

Hadron production in e^+e^- experiments is well described by the standard model of electroweak interactions, quantum chromodynamics and phenomenological models for the hadronization of quarks and gluons. It is highly desirable to also understand the transition of partons to hadrons in the framework of QCD.

ACKNOWLEDGEMENTS

I am grateful for the hospitality and support provided by the summer school organizers. My special thanks go to Janusz Kempa, Jerzy Wdowczyk and Wiesław Tkaczyk. I thank also Detlev Maier and Volker Schreiber for their help in preparing the written version of my talk.

REFERENCES

- [1] S. Bethke, Univ. Heidelberg, HD-PY 93/07 (1993).
- [2] M. Schmelling, *Phys. Scripta* **51** (1995) 683.
- [3] B. R. Webber, Cavendish-HEP, 94/17 (1994).
- [4] C. Grupen, *Particle Detectors*, Cambridge University Press, (1996).
- [5] OPAL Collaboration, R. Akers et al., CERN-PPE 95-21 (1995).
- [6] OPAL Collaboration, R. Akers et al., CERN-PPE 94-49 (1994).
- [7] ALEPH Collaboration, D. Decamp et al., *Phys. Lett. B* **273** (1991) 181.
- [8] OPAL Collaboration, R. Akers et al., *Z. Phys. C* **53** (1992) 539.
- [9] OPAL Collaboration, G. Alexander et al., CERN-PPE 96-47 (1996).
- [10] ALEPH Collaboration, D. Buskulic et al., CERN-PPE 96-43 (1996).
- [11] DELPHI Collaboration, P. Abreu et al., CERN-PPE 96-05 (1996) and *Phys. Lett. B* **372** (1996) 172.
- [12] L3 Collaboration, M. Acciarri et al., CERN-PPE 95-192 (1995) and *Phys. Lett. B* **371** (1996) 137.
- [13] Particle Data Group, M. Aguilar-Benitez et al., *Phys. Rev. D* **54** (1996) 1.
- [14] OPAL Collaboration, R. Akers et al., CERN-PPE 95-75 (1995).
- [15] ALEPH Collaboration, D. Buskulic et al., *Phys. Lett. B* **357** (1995) 487.

